Tilted-grating approach for scanning-mode X-ray phase contrast imaging

Arboleda, Carolina ; Wang, Zhentian ; Stampanoni, Marco

Abstract: Among the existent X-ray phase-contrast modalities, grating interferometry appears as a very promising technique for commercial applications, since it is compatible with conventional X-ray tubes and is robust from a mechanical point of view. However, since applications such as medical imaging and homeland security demand covering a considerable field of view, the fabrication of large-area gratings, which is known to be challenging and expensive, would be needed. A scanning setup is a good solution for this issue, because it uses cheaper line instead of large-area 2D detectors and, therefore, would require smaller gratings. In such a setup, the phase-retrieval using the conventional phase-stepping approach would be very slow, so having a faster method to record the signals becomes fundamental. To tackle this problem, we present a scanning-mode grating interferometer design, in which a grating is tilted to form Moiré fringes perpendicular to the grating lines. The sample is then translated along the fringes, so each line detector records a different phase step for each slice of the sample. This new approach was tested both in a simulated scenario and in an experimental setting, and its performance was quantitatively satisfactory compared to the traditional phase-stepping method and another existing scanning-mode technique.

DOI: https://doi.org/10.1364/OE.22.015447

Tilted-grating approach for scanning-mode X-ray phase contrast imaging

Carolina Arboleda,[1,2] **Zhentian Wang,**[1,2] **and Marco Stampanoni**[1,2,*]

[1]*Swiss Light Source, Paul Scherrer Institute, 5232 Villigen, Switzerland*
[2]*Institute for Biomedical Engineering, University and ETH Zurich, 8092 Zurich, Switzerland*
[*]*marco.stampanoni@psi.ch*

Abstract: Among the existent X-ray phase-contrast modalities, grating interferometry appears as a very promising technique for commercial applications, since it is compatible with conventional X-ray tubes and is robust from a mechanical point of view. However, since applications such as medical imaging and homeland security demand covering a considerable field of view, the fabrication of large-area gratings, which is known to be challenging and expensive, would be needed. A scanning setup is a good solution for this issue, because it uses cheaper line instead of large-area 2D detectors and, therefore, would require smaller gratings. In such a setup, the phase-retrieval using the conventional phase-stepping approach would be very slow, so having a faster method to record the signals becomes fundamental. To tackle this problem, we present a scanning-mode grating interferometer design, in which a grating is tilted to form Moiré fringes perpendicular to the grating lines. The sample is then translated along the fringes, so each line detector records a different phase step for each slice of the sample. This new approach was tested both in a simulated scenario and in an experimental setting, and its performance was quantitatively satisfactory compared to the traditional phase-stepping method and another existing scanning-mode technique.

OCIS codes: (340.7450) X-ray interferometry; (340.7440) X-ray imaging; (100.5070) Phase retrieval; (120.4120) Moire' techniques.

References and links

1. C. David, B. Nöhammer, H. H. Solak, and E. Ziegler, "Differential x-ray phase contrast imaging using a shearing interferometer," Appl. Phys. Lett. **81**, 3287 (2002).
2. A. Momose, S. Kawamoto, I. Koyama, Y. Hamaishi, K. Takai, and Y. Suzuki, "Demonstration of X-Ray Talbot interferometry," Jpn. J. Appl. Phys. **42**, L866–L868 (2003).
3. F. Pfeiffer, C. Kottler, O. Bunk, and C. David, "Hard X-ray phase tomography with low-brilliance sources," Phys. Rev. Lett. **98**, 108105 (2007).
4. E. Castelli, F. Arfelli, D. Dreossi, R. Longo, T. Rokvic, M. A. Cova, E. Quaia, M. Tonutti, F. Zanconati, A. Abrami, V. Chenda, R. H. Menk, E. Quai, G. Tromba, P. Bregant, and F. de Guarrini, "Clinical mammography at the SYRMEP beam line," Nucl. Instrum. Methods A **572**, 237–240 (2007).
5. N. Hauser, Z. Wang, R. Kubik-Huch, M. Trippel, G. Singer, M.K. Hohl, E. Roessl, T. Köhler, U. van Stevendaal, and N. Wieberneit, "A study on mastectomy samples to evaluate breast imaging quality and potential clinical relevance of differential phase contrast mammography," Invest. Radiol. **49**(3), 131–137 (2013).
6. E. Roessl, H. Daerr, T. Koehler, G. Martens, and U. van Stevendaal, "Clinical boundary conditions for grating-based differential phase-contrast mammography," Philos. Trans. R. Soc. London Ser. A **372**, 1–15 (2014).

#211218 - $15.00 USD Received 13 May 2014; revised 10 Jun 2014; accepted 10 Jun 2014; published 17 Jun 2014

7. M. Stampanoni, Z. Wang, T. Thüring, C. David, E. Roessl, M. Trippel, R. Kubik-Huch, G. Singer, M. K. Hohl, and N. Hauser, "The first analysis and clinical evaluation of native breast tissue using differential phase-contrast mammography," Invest. Radiol. **46**(12), 801–806 (2011).
8. D. Stutman, T. J. Beck, J. Carrino, and C. O. Bingham, "Talbot phase-contrast x-ray imaging for the small joints of the hand," Phys. Med. Biol. **56**, 5697–5720 (2011).
9. T. Thüring, R. Guggenberger, H. Alkadhi, J. Hodler, M. Vich, Z. Wang, C. David, and M. Stampanoni, "Human hand radiography using X-ray differential phase contrast combined with dark-field imaging," Skeletal Radiol. **42**(6), 827–835 (2013).
10. Z. Wang and M. Stampanoni, "Quantitative x-ray radiography using grating interferometry: a feasibility study," Phys. Med. Biol. **58**, 6815–6826 (2013).
11. T. Weitkamp, C. David, O. Bunk, J. Bruder, P. Cloetens, and F. Pfeiffer, "X-ray phase radiography and tomography of soft tissue using grating interferometry," Eur. J. Radiol. **68**, S13–S17 (2008).
12. T. Weitkamp, A. Diaz, C. David, F. Pfeiffer, M. Stampanoni, P. Cloetens, and E. Ziegler, "X-ray phase imaging with a grating interferometer," Opt. Express **12**(16), 6296–6304 (2005).
13. E. Roessl, H. Daerr, T. Koehler, G. Martens, and U. van Stevendaal, "Slit-scanning differential phase-contrast mammography: First experimental results," Proc. SPIE **9033**, 90330C (2014).
14. C. Kottler, F. Pfeiffer, O. Bunk, C. Grünzweig, and C. David, "Grating interferometer based scanning setup for hard X-ray phase contrast imaging," Rev. Sci. Instrum. **78**, 043710 (2007).
15. F. Pfeiffer, T. Weitkamp, O. Bunk, and C. David, "Phase retrieval and differential phase-contrast imaging with low-brilliance X-ray sources," Nat. Phys. **2**, 258–261 (2006).
16. C. David and F. Pfeiffer, "X-ray interferometer for phase contrast imaging," Patent WO 2008/006470 A1 (17. Jan, 2008).
17. S. A. McDonald, F. Marone, C. Hintermüller, G. Mikuljan, C. David, F. Pfeiffer, and M. Stampanoni, "Advanced phase-contrast imaging using a grating interferometer," J. Synchrotron Rad. **16**, 562–572 (2009).
18. T. Thuering, P. Modregger, T. Grund, J. Kenntner, C. David, and M. Stampanoni, "High resolution, large field of view x-ray differential phase contrast imaging on a compact setup," Appl. Phys. Lett. **99**, 041111 (2011).
19. C. Arboleda, Z. Wang, and M. Stampanoni, "Wavelet-based noise-model driven denoising algorithm for differential phase contrast mammography," Opt. Express **21**, 10572–10589 (2013).
20. M. P. Sampat, Z. Wang, S. Gupta, A. C. Bovik, and M. K. Markey, "Complex wavelet structural similarity: a new image similarity index," IEEE Trans. Image Proc. **18**, 2385–2401 (2009).
21. F. Pfeiffer, M. Bech, O. Bunk, P. Kraft, E. F. Eikenberry, C. Brönnimann, C. Grünzweig, and C. David, "Hard-X-ray dark-field imaging using a grating interferometer," Nat. Mater. **7**, 134–137 (2008).
22. G. Lovric, P. Oberta, I. Mohacsi, M. Stampanoni, and R. Mokso, "A robust tool for photon source geometry measurements using the fractional Talbot effect," Opt. Express **22**, 2745–2760 (2014).
23. T. J. Suleski, "Generation of Lohmann images from binary-phase Talbot array illuminators," Appl. Opt. **36**, 4686–4691 (1997).
24. T. Thüring, "Compact X-ray grating interferometry for phase and dark-field computed tomography in the diagnostic energy range," PhD thesis, ETH Zurich (2013).
25. Precision Linear Stages LTM 80, OWIS GmbH, www.owis.eu.

1. Introduction

Grating interferometry [1-3] constitutes a very promising technique for commercial X-ray phase-contrast applications, since it works with traditional X-ray tubes, is mechanically robust and has modest requirements for monochromaticity and spatial coherence. In the last few years, several exciting applications of this technique have been reported, ranging from material inspection to medical imaging [4-11].

To carry out the transition of grating interferometry from the laboratory to the commercial setting, it has to be tailored to cover a large field of view (FOV) and allow reasonable exposure times. To fulfill these requirements, a scanning setup would be an excellent choice, since it requires line instead of 2D detectors and would avoid the fabrication of large-area gratings, which might be laborious and pricy [6]. On the other hand, in order to retrieve different contrast signals, conventional grating interferometry requires a phase-stepping procedure [12], in which one of the gratings is translated stepwise (in sub-micron scale) and an image is acquired for each step. This procedure is time-consuming in general and demands high system stability and accuracy, so it constitutes a major problem for the implementation of grating interferometry in a commercial setting. A scanning-mode method able to "hard-code" the phase-stepping

#211218 - $15.00 USD Received 13 May 2014; revised 10 Jun 2014; accepted 10 Jun 2014; published 17 Jun 2014

procedure into a one-dimension scan [13], can fundamentally solve the problem.

In this regard, Kottler et al [14] introduced a scanning-mode grating interferometry setup. They proposed a method in which a Moiré fringe parallel to the grating lines is generated by slightly changing the theoretical inter-grating distance. In this arrangement, equidistantly distributed lines of the detector correspond to different relative positions of the phase and absorption gratings, which can be regarded as phase-steps. Therefore, by translating the sample in a direction perpendicular to the fringe orientation, a phase-stepping curve can be retrieved and Fourier-Component Analysis (FCA) [15] can be used to reconstruct the signals.

Another possibility to solve this issue is to use a staggered grating, so that the grating is located at a different lateral position for each line detector, and a phase stepping curve can be retrieved by scanning the sample in a direction perpendicular to the grating lines [16]. However, this approach implies the fabrication of gratings with a novel design which will be hard to align, and kept as such, with the line detectors. As an alternative to this technique, we propose a tilted-grating-based scanning method for grating interferometry. The idea is to generate a Moiré fringe perpendicular to the grating lines by tilting one of the gratings, so that each line detector ends up recording a different phase step as the sample is translated. This method was tested by conducting simulations and performing experiments on a Talbot interferometer [17-18]. Its outcomes were compared to those yielded by the traditional phase-stepping technique and Kottler's method, and proved to be quantitatively accurate according to the Complex Wavelet Structural Similarity (CW-SSIM) index [19-20].

2. Tilted-grating design

A standard grating interferometer is shown in Fig. 1, where G0, G1 and G2 are the source, phase and absorption gratings, respectively. The use of G0 is optional, depending on the spatial coherence properties of the X-ray source [15]. The idea behind the tilted-grating design is illustrated in Fig. 2.

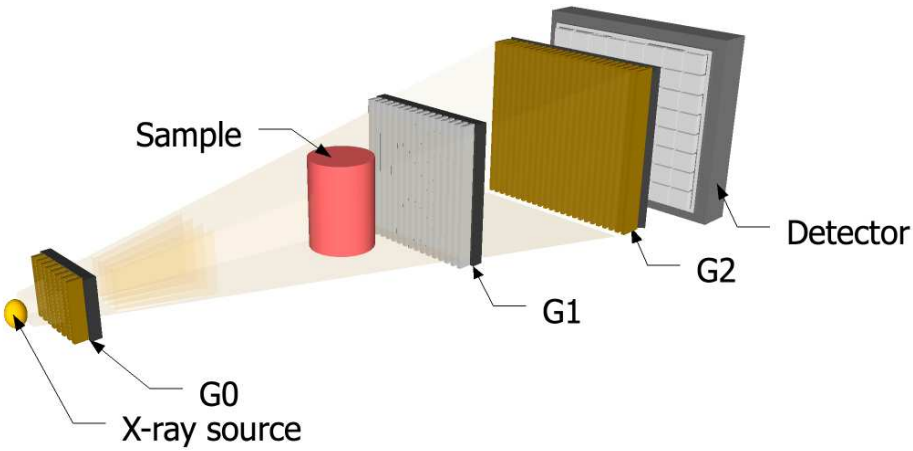

Fig. 1. Sketch of an X-ray grating interferometer.

If we have a staggered grating [Fig. 2(a)] [16], such that each line detector is covered by the grating at a different position in x direction, we can mimic the phase-stepping approach by scanning the sample along y direction, without the need of moving G2, and will end up having each line detector record a different phase step for each slice of the sample, as long as the grating lines are subsequently shifted by a distance δ_x, defined as:

#211218 - $15.00 USD Received 13 May 2014; revised 10 Jun 2014; accepted 10 Jun 2014; published 17 Jun 2014

$$\delta_x = m\frac{p_2}{n}, \tag{1}$$

where n is the number of line detectors, so that the whole staggered grating is covering an integer number m of periods p_2 of G2. Since the fabrication of this staggered grating and its successive alignment to the corresponding line detectors might become very challenging, an easier way to achieve the same effect is to tilt G2, as shown in Fig. 2(b). Assuming our line detectors are separated by a distance D, the tilting angle θ can be calculated as:

$$\theta = arctan\left(\frac{\delta_x}{D}\right), \tag{2}$$

To compensate for the beam divergency, the sample-translation step s must be adjusted to:

$$s = D\frac{L}{L+d}, \tag{3}$$

where L is the source-to-G1 distance and d represents the inter-grating distance. Afterwards, the absorption, DPC and dark-field signals can be retrieved by standard FCA. A reference image (i.e. no sample in the beam) has to be acquired as well in order to subtract the background phase distribution, like in the phase-stepping approach [12].

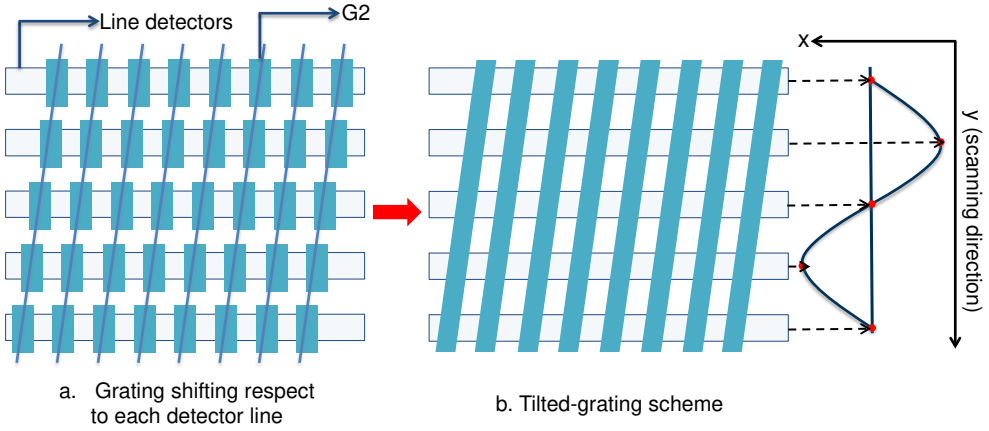

Fig. 2. Tilted-grating method. a. Sketch of a staggered grating, where the grating at a different lateral position covers each detector line. b. To achieve the same effect, the grating is tilted so that each line detector records a different phase step (red dots on the phase-stepping curve shown on the right).

Recapitulating, we start the procedure by calculating the tilting angle based on our hardware (i.e. the number of line detectors and the separation between them) and the number of periods p_2 we want to cover. Subsequently, we tilt G2 and acquire a reference image to be able to retrieve a background phase-stepping curve. Afterwards, we move our sample along y direction (see Fig. 2) by successive steps s until the signal corresponding to each slice has been recorded by the number of line detectors used for the calculations, so that a sample phase-stepping curve for each slice can be retrieved. Rearranging the acquired data, the absorption, DPC and dark-field signals can be reconstructed by performing FCA in two dimensions.

#211218 - $15.00 USD Received 13 May 2014; revised 10 Jun 2014; accepted 10 Jun 2014; published 17 Jun 2014

3. Simulations

To test the working principle of our approach, a Talbot-Lau grating interferometer [3, 21] that could fit into a commercial apparatus was simulated [6]. The Fresnel diffraction integral was used to propagate the spherical wave between the gratings from the source to the detector as described in [22]. To simplify the calculations, a monochromatic source and ideal gratings were assumed. The pitches for G0, G1 and G2 were 61.5 μm, 1.97 μm and 1 μm, respectively, and their duty cycle was 50 %. The energy was 25 keV, the total length of the interferometer was 62 cm and the inter-grating distance was 9.92 mm, which corresponds to the first Talbot order [23] in this arrangement. The sample was a non-scattering PMMA sphere ($\delta = 4.5 \times 10^{-7}$, $\beta = 6.8 \times 10^{-11}$) of radius 120 μm. For the phase-stepping method, an area detector of 63 $\times$ 63 pixels with a pixel size of 4 μm $\times$ 4 μm was simulated and 12 phase steps were performed; for the scanning-mode methods, a detector with 12 lines was simulated. Each line contained 63 pixels with a pixel size of 4 μm $\times$ 4 μm and the separation between lines was set to 8 μm. The same total exposure times were used for all three methods. All the simulations were implemented in Matlab.

4. Experimental setup

4.1. Grating interferometer

A 1.1 m long Talbot interferometer [24] operated at 25 keV was used for our measurements. A micro-focus X-ray source (HAMMAMATSU L10101) with a 5 μm focal-spot size was employed. The source-to-G1 distance and the inter-grating distance (third Talbot order) were L=88.19 cm and d=21.81 cm, respectively. The gratings (Microworks GmbH, Germany) had a duty cycle of 50 %; G1 was made of silicon and had a pitch of 4.81 μm, while G2 was made of gold and had a period of 3 μm. The detector was a CCD camera (PI-SCX:4300, Princeton Instruments) with an active area of 50 mm $\times$ 50 mm, a pixel size of 24 μm and a dynamic range of 16 bits. For the conversion of X-rays to visible light, it uses a $Gd_2O_2S:Tb$ (Gadox) scintillator, which has a resolution of 60 to 80 μm [24]. A binning factor of 2 was applied in order to reduce the detector read-out time and increase the signal-to-noise ratio (SNR). For all the methods, exposure times of up to 60 s per phase step and varying numbers of phase steps were tested out. However, for the comparisons, the total exposure time was kept constant. These long exposure times were required, because we had a micro-focus source and a long setup.

It is important to point out that we used this setup only for demonstration. For commercial applications, we would need a much more compact setup with a larger X-ray source, as the one we simulated.

4.2. Imaging protocol

A polyethylene double-layer Eppendorf tube and a mouse head were scanned. Total exposure times of 50 and 61 minutes were used, respectively. The exposure time per step was varied in each method, in order to keep the total exposure time, and therefore the dose, constant. Five dark-current scans were carried out at the beginning of each acquisition, so the average dark-current signal could be subtracted from the reference and sample scans before the reconstruction. For both scanning-mode methods, five reference images were acquired and averaged during the background phase-stepping-curve retrieval.

For the phase-stepping method, the phantom and the mouse head were scanned using 23 and 58 phase steps, respectively. To perform the tilted-grating technique, the angle θ (Eq. (2)) was adjusted so one period of the G2 grating was scanned ($m = 1$). For the phantom, 40 scanning steps were performed, each of 307 μm, to scan each slice of the sample with detector rows separated by 384 μm, so $\theta = 195$ μrad; for the mouse head, 112 steps of 38.5 μm each were

#211218 - $15.00 USD Received 13 May 2014; revised 10 Jun 2014; accepted 10 Jun 2014; published 17 Jun 2014

carried out, to record the signals with detector rows separated by 48 μm, so $\theta = 558$ μrad.

For Kottler's method, the inter-grating distance was increased by 1% of the Talbot distance, i.e. 2.18 mm, and the Moiré fringe was checked beforehand in order to determine the appropriate scan step size and number of steps to get an integer number of fringe periods covered. For the phantom, 56 steps of 38.5 μm each were performed, to cover two fringe periods and record the signals with detector columns separated by 48 μm. For the biological sample, 112 steps of 38.5 μm as well were carried out, so that 4 periods of the Moiré fringe were scanned.

The Moiré fringes produced for both scanning-mode methods during the acquisition of the phantom images are shown in Fig. 3. As explained above, the tilted-grating method generates fringes perpendicular to the grating lines, while Kottler's produces fringes in a parallel orientation.

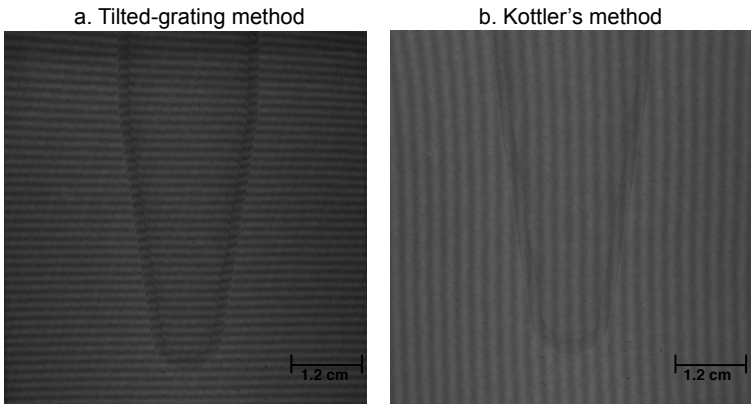

Fig. 3. Moiré fringes generated for the tilted-grating and Kottler's methods, during the acquisition of the phantom images.

5. Image quality assessment

For both the simulated and experimental data, the Complex Wavelet Structural Similarity (CW-SSIM) index was used to evaluate the outcomes and the phase-stepping results were set as the ground truth. The CW-SSIM might be more informative than the widely used mean square error (MSE), as it does not only take into account the overall average difference in intensity values, but also the structural distortions. It assumes that only relative phase discrepancies between the sets of wavelet coefficients of two images yield significant structural differences the human visual system is sensitive to. This index goes from 0 to 1 and the larger it is, the more similar the images being compared [19-20]. However, since the simulated phantom was a sphere and the potential structural distorsions are not very meaningful for this kind of sample, the MSE was computed as well in this case, to get a better idea of the accuracy of both methods.
In addition, for the experimental data, the SNR was calculated as the ratio of the mean and standard deviation in a region of interest (ROI) inside the object.

6. Results and discussion

The DPC images reconstructed from simulated data are shown in Fig. 4 and the corresponding MSE and CW-SSIM values are reported in Table 1. According to the CW-SSIM, both methods proved to be quantitatively accurate and there was no significant difference between their

#211218 - $15.00 USD Received 13 May 2014; revised 10 Jun 2014; accepted 10 Jun 2014; published 17 Jun 2014

performances [20]. The MSE favored the tilted-grating method for the DPC signal, but it is important to take into account that the random noise contributed to this error. Since talking about structural distorsions for this kind of sample is not very meaningful, the MSE can be regarded as a better performance index in this case.

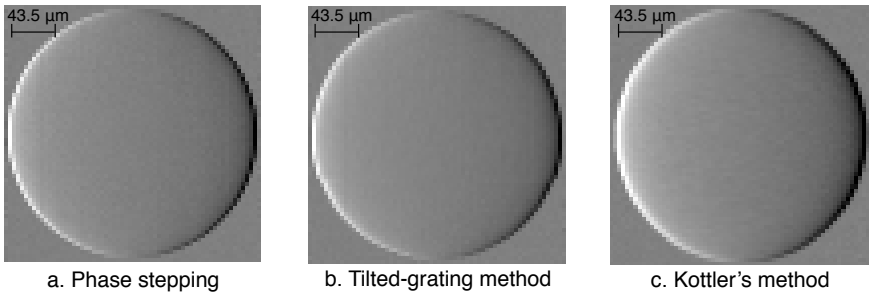

Fig. 4. DPC images reconstructed from simulated data. Both scanning-mode methods proved to be able to retrieve accurate DPC signals. Detector noise was included in the simulations.

Table 1. CW-SSIM and MSE values between the scanning-mode methods and the phase stepping technique for the simulated signals. Both scanning-mode methods proved to be quantitatively accurate, but the tilted-grating method yielded a MSE value much lower than Kottler's for the DPC signal.

Image type	CW-SSIM Kottler	CW-SSIM tilted	MSE Kottler	MSE tilted
Absorption	9.99e-1	9.99e-1	1.52e-4	2.10e-5
DPC	9.92e-1	9.99e-1	1.89e-3	1.78e-4

Table 2. CW-SSIM values between the scanning-mode methods and the phase-stepping technique for the Eppendorf tube images. The values yielded by the tilted-grating technique are superior to Kottler's for all three signal types. As mentioned above, the tilted-grating and Kottler's signals were recorded with one and two periods, respectively, but with the same total exposure time.

Signal	CW-SSIM Kottler	CW-SSIM tilted
Absorption	9.95e-1	9.97e-1
DPC	8.72e-1	9.69e-1
Dark field	5.15e-1	7.82e-1

The reconstructed experimental phantom images are shown in Fig. 5 and the row profiles at the position marked by the red line are plotted in Fig. 6. The corresponding metrics (CW-SSIM, SNR) are reported in Table 2 and Table 3. As can be grasped from the former table, our method yielded higher CW-SSIM values and visually nicer images than Kottler's for all three types of signals, providing a particularly substantial increase in this metric for the DPC and dark-field data. Regarding the SNR, both scanning-mode methods provided higher values than phase stepping for all three signals and the tilted-grating method yielded the highest values for the DPC and dark-field images. These increases in SNR mean that these techniques have noise reduction

#211218 - $15.00 USD Received 13 May 2014; revised 10 Jun 2014; accepted 10 Jun 2014; published 17 Jun 2014

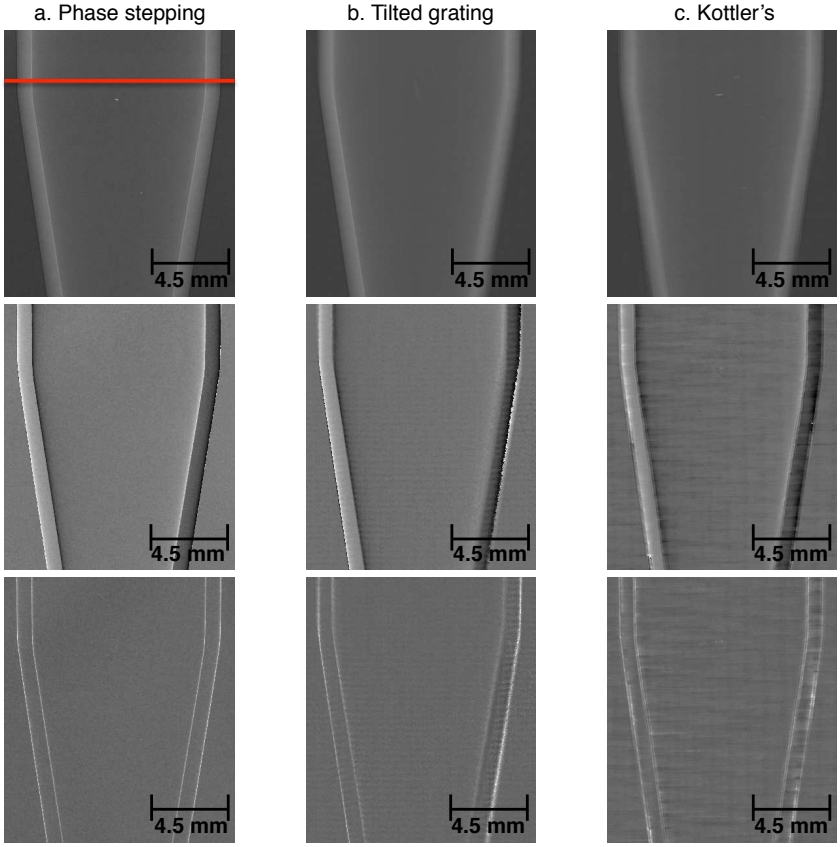

Fig. 5. Images of a plastic double-layer Eppendorf tube acquired with a total exposure time of 50 minutes. From top to bottom: Absorption, DPC and dark-field. Both scanning-mode methods yielded reasonable outcomes, but the visual quality of the images acquired with the tilted-grating technique is higher. However, there is some blurring present in these images, which we believe is due to the fact of lacking a stable sample translation stage. Row profiles for all the images corresponding to the position marked by the red line are plotted in Fig. 6.

capabilities, but, on the other hand, the smoothing caused by them could obscure some high-resolution features. In fact, we observe some blurring in the outcomes of these methods, and we attribute this effect to two possible causes. First of all, as the sample was translated, the gratings might have shifted as a consequence of the movement of the sample. Second, our sample holder was not ideal, since the sample was held from the top end only (i.e. it was hanging), so during the acquisition of the images it could have had small movements in directions other than the scanning direction. The latter affected the tilted-grating method more than Kottler's, since the sample was moved from top to bottom in that case. By having the possibility of fixing the sample on both ends, one expects the blurring to be significantly reduced. An alternative to reduce this artifact is to correct for the displacements produced in directions other than the scanning direction. After checking the recorded images, we realized there had been displacements in the direction perpendicular to the scanning direction of up to 7 pixels (i.e. 0.336 mm). Thus, we

#211218 - $15.00 USD Received 13 May 2014; revised 10 Jun 2014; accepted 10 Jun 2014; published 17 Jun 2014

displaced the images back to the position they should be in this direction and carried out the signal retrieval algorithm. This simple procedure proved to be effective to sharpen the edges, as it is evidenced in Fig. 7. We did not perform corrections in any other directions, because they could affect the phase-stepping curves.

Table 3. SNR values for the Eppendorf tube images. The tilted-grating method yielded the highest SNR values for the DPC and dark-field signals, while Kottler's produced the highest SNR for the absorption image.

Signal	SNR phase stepping	SNR Kottler	SNR tilted
Absorption	19.02	31.86	22.29
DPC	36.93	37.51	39.06
Dark field	4.79	7.84	9.84

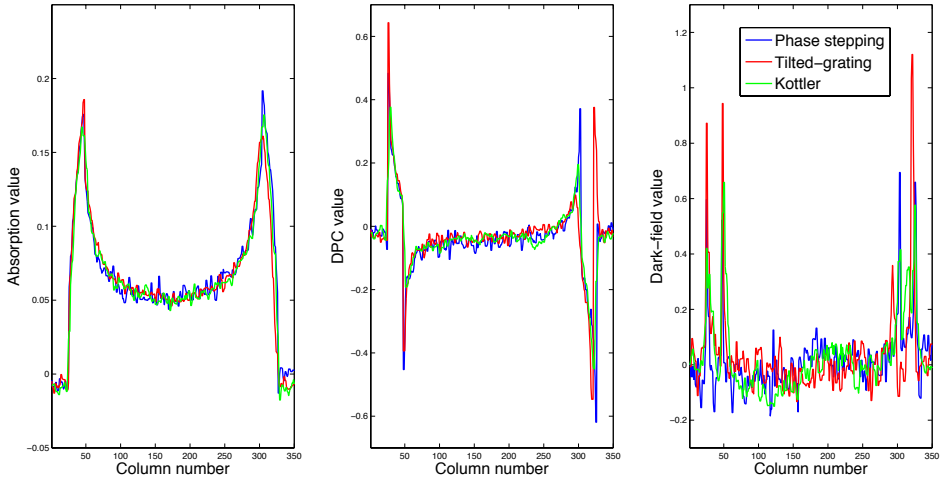

Fig. 6. Row profiles of a plastic double-layer Eppendorf tube acquired with a total exposure time of 50 minutes. Comparison between phase stepping and the two scanning-mode methods implemented. From left to right: Absorption, DPC and dark-field. The quantitative accuracy of our technique can be appreciated.

The mouse head images are depicted in Fig. 8 and the corresponding metrics are in Table 4. According to these values, our method outperformed Kottler's for the DPC and dark-field signals and had a comparable performance for absorption. The blurring effect discussed above is even more noticeable for this sample, since it contains smaller features. However, as already pointed out, we believe that a better translation stage, either for the sample or the imaging system, will solve this issue.

It is also important to comment on the gridding artifacts present in Kottler's images. We believe that the main cause of these artifacts is the fact that to carry out Kottler's method, the inter-grating distance is modified by a small percentage and the random-period Moiré fringes produced have to be checked in order to determine the scan step size and the number of scanning steps to cover an integer number of periods. This process is somehow operator-dependent and could lead to inevitable errors. Conversely, the tilted-grating method relies on the idea of mimicking a staggered grating and allows the automatic determination of the desired period of

#211218 - $15.00 USD Received 13 May 2014; revised 10 Jun 2014; accepted 10 Jun 2014; published 17 Jun 2014

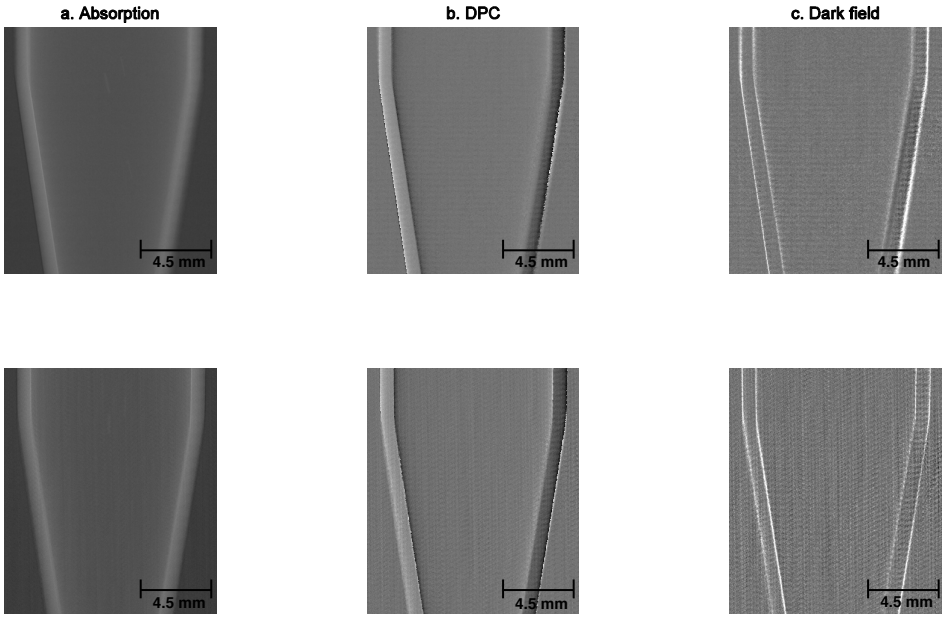

Fig. 7. Images of a plastic double-layer Eppendorf tube acquired with the tilted-grating method (top) and deblurred by registration of the images in one direction (bottom). The edges are better defined in the latter, proving the usefulness of this simple deblurring procedure.

the Moiré fringes by calculating the tilting angle through Eq. (1) and Eq. (2). Therefore, it is not operator-dependent and this constitutes an advantage over Kottler's method.

Another important point is the accuracy of the sample translation stage. According to the manual, the positioning error of this stage is up to 25 μm for each 100 mm, i.e. 0.025 % in both directions [25]. Although this error translates into very tiny inaccuracies in the movement of the sample in both directions, it adds up and can affect the precision of the scanning of the fringes. A possible solution to this issue, as well as to the one mentioned in the paragraph above, is to handle the fringe period error in the reconstruction. This correction might increase the computation time, but it could help to the improvement of the results presented here.

The phase-wrapping effect was highly reduced in the tilted-grating outcomes, but even more pronounced in Kottler's. This can be explained by the fact that the sample was translated laterally (along x direction) during Kottler's acquisition and this direction is more sensitive to changes in the refraction angle, as the grating lines are oriented perpendicularly to the sample translation direction. Notwithstanding, the phase-wrapping seems to give a visual impression that the edges are better defined in Kottler's DPC images (see Fig. 8(c)).

Table 4. CW-SSIM values between the scanning-mode methods and the phase-stepping technique for the mouse head images. The performance of the tilted-grating method was superior in the case of the dark-field and DPC signals.

Image type	CW-SSIM Kottler	CW-SSIM Tilted grating
Absorption	9.92e-1	9.88e-1
DPC	6.49e-1	9.00e-1
Dark field	5.15e-1	8.94e-1

#211218 - $15.00 USD Received 13 May 2014; revised 10 Jun 2014; accepted 10 Jun 2014; published 17 Jun 2014

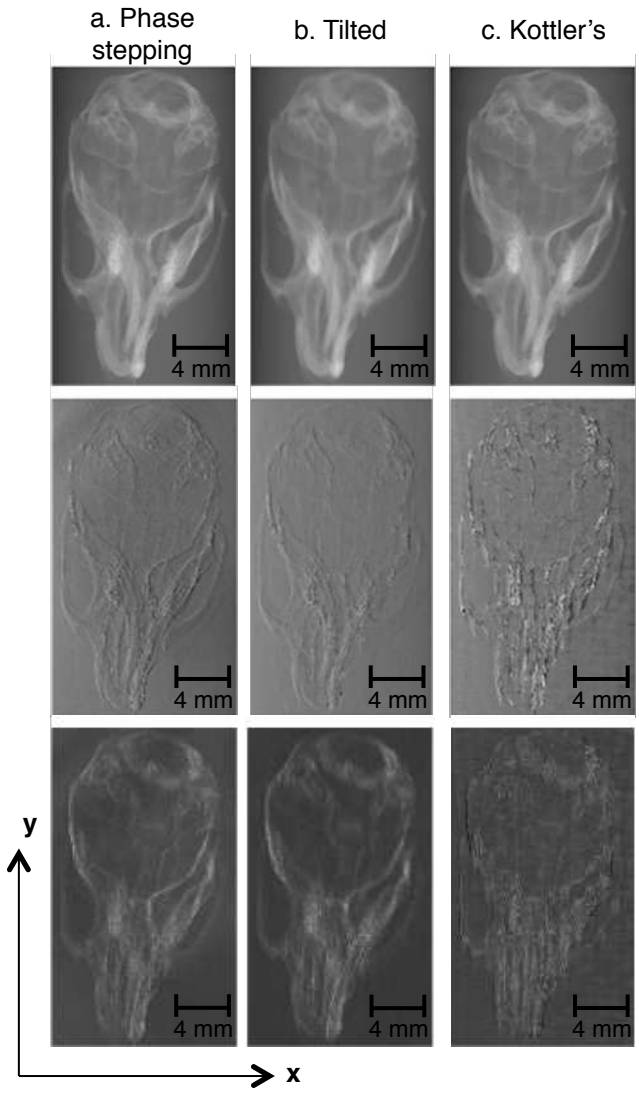

Fig. 8. Images of a mouse head. From top to bottom: Absorption, DPC and dark-field. Both scanning-mode methods yielded reasonable outcomes, but the tilted-grating method produced visually nicer images than Kottler's.

An issue concerning our experimental setup is the X-ray flux. We used a micro-focus source and, therefore, had to use long exposure times in order to get signals with enough SNR. However, by counting on a larger-focal-spot source (i.e. 300 μm, as in typical mammography machines) and using G0 to achieve the required spatial coherence, the exposure times could be reduced up to 100-fold [6].

Both scanning-mode methods exhibit higher demands than the phase-stepping approach on the alignment of the gratings, in order to be able to yield a straight-oriented Moiré fringe; in the case of the tilted-grating design, also to manage to achieve a precise rotation center. Another important point for these techniques is the separation between line detectors, because it limits the sample-translation step. The smaller this step, the finer the sampling of the phase-stepping

#211218 - $15.00 USD Received 13 May 2014; revised 10 Jun 2014; accepted 10 Jun 2014; published 17 Jun 2014

curves and, thus, the higher the image quality.

Although there is no difference in the required accuracy of the fringe patterns between both scanning-mode methods, the fundamental difference stems from the way of generating the Moiré fringes, as we stated above. We believe that the implementation of the tilted-grating method is much straightforward than Kottler's method in practice, as there is a simple way to automatically generate a Moiré fringe of a desired period. Moreover, there is a clear theoretical motivation behind our method, which is to mimic a staggered grating, and additionally the gratings are at the design position (Talbot distance) of the grating interferometer, therefore the system maintains an optimal visibility of the phase-stepping curve (important to image quality). For Kottler's method, it is difficult to control the period of the Moiré fringe, usually a random-period Moiré fringe is produced by misaligning one of the gratings along the beam direction, and afterwards the scan step size and the number of steps have to be adjusted in order to be able to scan an integer number of fringe periods. Due to the mismatch of the grating positions in Kottler's method, the gratings are not at the optimal position, which potentially leads to a loss in fringe visibility (detrimental to image quality) and therefore limits the flexibility to tune the fringe period.

7. Conclusion

It was demonstrated that the tilted-grating design presented here allows the retrieval of absorption, DPC and dark-field signals comparable to the outcomes of conventional X-ray phase-contrast grating interferometry. In addition, it proved to be relatively easy to implement in practice, as good-quality, small-size gratings are already available. This method requires good motors to align and rotate the gratings at least once, as well as a precise and mechanically-robust scanning stage to either move the sample or the whole system as it would be required in applications such as mammography [6]. In addition, the separation between line detectors plays an important role too, because it constrains the length of the scanning step, and the smaller this step, the finer the sampling of the fringes.

From the comparison between the proposed tilted-grating technique and Kottler's method, it can be said that the fact that the former allows the generation of a fringe with a desired period through the computation of a specific tilting angle and, additionally, avoids the modification of the G1-G2 distance, constitutes an advantage over Kotler's, since the latter implies the modification of this inter-grating separation, which can become detrimental for the visibility. However, it is important to point out that the errors in the fringe period determination produced in Kottler's method might be corrected in the reconstruction algorithm, but at the expense of longer computation times.

It is also important to emphasize that the tilted-grating method does not require the fabrication of any special gratings, which constitutes a big advantage, since it can be implemented with conventional absorption and phase gratings without the need of incurring in any additional costs for this matter. To demonstrate the actual feasibility of our technique for commercial applications, we will have to test it in a experimental setting where the imaging system, instead of the sample, is moved to perform the scanning. However, we are confident that it will perform well in this scenario.

Acknowledgments

The authors thank Thomas Thüring for building the experimental setup, Gordan Mikuljan for his help during measurements and Alberto Astolfo for the supply of the biological sample. They also acknowledge the assistance of Matias Kagias and Goran Lovric with the simulations. Part of this work has been supported by the ERC Grant ERC-2012-StG 310005-PhaseX and the National Competence Center for Biomedical Imaging (NCCBI).

#211218 - $15.00 USD Received 13 May 2014; revised 10 Jun 2014; accepted 10 Jun 2014; published 17 Jun 2014